PCCP

PAPER

View Article Online
View Journal | View Issue

Cite this: *Phys. Chem. Chem. Phys.*, 2017, **19**, 28153

Enhancing the resolution of ^{1}H and ^{13}C solid-state NMR spectra by reduction of anisotropic bulk magnetic susceptibility broadening†

Michael P. Hanrahan,[ab] Amrit Venkatesh,[ab] Scott L. Carnahan,[ab] Julie L. Calahan,[c] Joseph W. Lubach,[d] Eric J. Munson*[c] and Aaron J. Rossini*[ab]

We demonstrate that natural isotopic abundance 2D heteronuclear correlation (HETCOR) solid-state NMR spectra can be used to significantly reduce or eliminate the broadening of ^{1}H and ^{13}C solid-state NMR spectra of organic solids due to anisotropic bulk magnetic susceptibility (ABMS). ABMS often manifests in solids with aromatic groups, such as active pharmaceutical ingredients (APIs), and inhomogeneously broadens the NMR peaks of all nuclei in the sample. Inhomogeneous peaks with full widths at half maximum (FWHM) of ~1 ppm typically result from ABMS broadening and the low spectral resolution impedes the analysis of solid-state NMR spectra. ABMS broadening of solid-state NMR spectra has previously been eliminated using 2D multiple-quantum correlation experiments, or by performing NMR experiments on diluted materials or single crystals. However, these experiments are often infeasible due to their poor sensitivity and/or provide limited gains in resolution. 2D ^{1}H–^{13}C HETCOR experiments have previously been applied to reduce susceptibility broadening in paramagnetic solids and we show that this strategy can significantly reduce ABMS broadening in diamagnetic organic solids. Comparisons of 1D solid-state NMR spectra and ^{1}H and ^{13}C solid-state NMR spectra obtained from 2D ^{1}H–^{13}C HETCOR NMR spectra show that the HETCOR spectrum directly increases resolution by a factor of 1.5 to 8. The direct gain in resolution is determined by the ratio of the inhomogeneous ^{13}C/^{1}H linewidth to the homogeneous ^{1}H linewidth, with the former depending on the magnitude of the ABMS broadening and the strength of the applied field and the latter on the efficiency of homonuclear decoupling. The direct gains in resolution obtained using the 2D HETCOR experiments are better than that obtained by dilution. For solids with long proton longitudinal relaxation times, dynamic nuclear polarization (DNP) was applied to enhance sensitivity and enable the acquisition of 2D ^{1}H–^{13}C HETCOR NMR spectra. 2D ^{1}H–^{13}C HETCOR experiments were applied to resolve and partially assign the NMR signals of the form I and form II polymorphs of aspirin in a sample containing both forms. These findings have important implications for ultra-high field NMR experiments, optimization of decoupling schemes and assessment of the fundamental limits on the resolution of solid-state NMR spectra.

Received 22nd June 2017,
Accepted 25th September 2017

DOI: 10.1039/c7cp04223j

rsc.li/pccp

Introduction

Solid-state NMR is a widely applied tool for the characterization of solid materials such as active pharmaceutical ingredients (APIs).[1–4] However, the analysis of solid-state NMR spectra is often impeded by their low spectral resolution. One mechanism that frequently reduces the resolution of solid-state NMR spectra of organic solids and APIs is anisotropic bulk magnetic susceptibility (ABMS) broadening.[5–8] For samples affected by ABMS the full widths at half maximum (FWHM) of peaks in ^{13}C solid-state NMR spectra are often on the order of 1 ppm,[5–8] even in highly crystalline samples. This broadening often arises in APIs and organic solids that contain aromatic groups because the magnetic susceptibility is anisotropic; this means that the susceptibility, the induced magnetic field, and consequently the isotropic chemical shift for a given crystallite in a powder depends on its orientation with respect to the external magnetic field and the orientations of the neighboring crystallites.[5–9]

[a] *Iowa State University, Department of Chemistry, Ames, 50011, IA, USA. E-mail: arossini@iastate.edu*
[b] *US DOE Ames Laboratory, Ames, Iowa, 50011, USA*
[c] *University of Kentucky, College of Pharmacy, Lexington, Kentucky, 40536, USA. E-mail: eric.munson@uky.edu*
[d] *Genentech, Inc., Department of Small Molecule Pharmaceutical Sciences, 1 DNA Way, South San Francisco, CA, 94080, USA*

† Electronic supplementary information (ESI) available: Additional solid-state NMR spectra, results of plane-wave DFT calculations, data analysis and details of spectral processing. See DOI: 10.1039/c7cp04223j

ABMS often causes substantial inhomogeneous broadening of the resonances of all nuclei in the sample (^{1}H, ^{13}C, ^{15}N, ^{31}P, *etc.*). Increasing the strength of the applied field often does not improve the resolution of 1D ^{1}H and ^{13}C solid-state NMR spectra because ABMS broadening is inhomogeneous (constant in ppm).

ABMS broadening was first observed in the solid-state in the early days of high resolution solid-state NMR.[5,6] Garroway and co-workers observed and predicted many of the effects of ABMS broadening on solid-state NMR spectra: magic angle spinning (MAS) cannot eliminate ABMS broadening; when ABMS is the dominant broadening mechanism, all ^{13}C lines are broadened to similar extents; solids with aromatic groups are likely to be most strongly affected by ABMS due to ring currents; and ABMS broadening can be reduced by diluting the sample in a material with isotropic magnetic susceptibility.[5] It has also been demonstrated that solid-state NMR experiments on single crystals can reduce ABMS broadening.[10,11] Hexamethylbenzene (HMB) is the prototypical sample displaying ABMS broadening; both the methyl and aromatic carbon ^{13}C peaks have FWHM greater than 1 ppm, and the FWHM of the peaks (in ppm) are independent of the applied field (*vide infra*).[5,6,12] Substantial ABMS broadening has also been clearly observed in the ^{13}C solid-state NMR spectra of porphyrins,[10] glycine,[11] metal–organic frameworks (MOF),[13] APIs with aromatic groups such as ibuprofen[7] and piroxicam HCl;[14] in the ^{19}F solid-state NMR spectrum of octafluoronaphthalene[8] and in the high resolution ^{1}H solid-state NMR spectra of organic materials obtained using combined rotation and multiple pulse spectroscopy (CRAMPS)[15] or ultrafast MAS ($\nu_r > 100$ kHz).[16,17] Paramagnetic materials also often show substantial susceptibility broadenings which can be on the order of 10 ppm.[18] We were also able to identify several other solid-state NMR studies of APIs/organic solids containing aromatic rings where there is likely substantial ABMS broadening present;[19–21] however, the ABMS broadening is not acknowledged or commented upon. Even in crystalline samples free of aromatic groups, ABMS broadening is predicted to be the ultimate factor that limits resolution under high magnetic fields,[22] or when ultrafast MAS is applied to directly acquire ^{1}H solid-state NMR spectra.[17] It is possible to calculate the magnetic susceptibility tensor using plane-wave DFT calculations and predict the magnitude of the ABMS broadening when the solid-state structure is known.[8]

A number of solution and solid-state NMR methods have been proposed to eliminate or reduce susceptibility broadening, broadening due to inhomogeneous magnetic fields, or even broadening due to structural disorder.[8,23–39] Emsley and co-workers[37,38] and others[8,16] have previously shown that 2D double quantum–single quantum (DQ–SQ) or zero quantum–single quantum (ZQ–SQ) correlation solid-state NMR spectra can be used to reduce inhomogeneous broadening in solids due to susceptibility effects. ABMS will normally shift the resonances of the correlated spins observed in a DQ–SQ spectrum by the same amount, leading to ''correlated inhomogeneous broadening'', where the inhomogeneous broadening is dispersed along elongated/tilted cross-peaks that have slopes determined by the coherence order ratios.[37,38] The ABMS broadening is then reduced or eliminated in the individual rows or columns of the 2D DQ–SQ spectrum. Alternatively, the 2D DQ–SQ spectrum may be sheared to obtain a ZQ–SQ NMR spectrum with reduced susceptibility broadening and improved resolution.[37,38] In some favorable instances, inhomogeneous broadening due to structural disorder can also be reduced or eliminated in a 2D DQ–SQ spectrum.[37,38] Unfortunately, 2D ZQ–SQ/DQ–SQ homonuclear correlation solid-state NMR experiments with natural abundance ^{13}C are very challenging since sensitivity will be reduced by a factor of more than 100 compared to a standard 1D NMR spectrum. Therefore, alternative strategies for eliminating broadening due to ABMS are required.

Heteronuclear correlation (HETCOR) experiments have previously been used to reduce susceptibility broadening in solution NMR experiments.[23] Emsley and co-workers showed that the inhomogeneous paramagnetic susceptibility broadening on the order of 10 ppm observed in an iron complex could be significantly reduced using 2D ^{1}H–^{13}C HETCOR solid-state NMR experiments.[18] 2D HETCOR experiments can reduce susceptibility broadening because heteronuclear spin pairs will experience the same local magnetic field. The resonance frequencies of correlated spin pairs will be shifted by the same amount, which leads to correlated inhomogeneous broadening in a 2D spectrum.[23] Susceptibility broadening then manifests as elongated/tilted cross-peaks in a 2D HETCOR spectrum.[18] The individual rows/columns of the 2D HETCOR spectrum will then show enhanced resolution as compared to the corresponding projections or 1D spectra (*vide infra*).[18] Dybowski and co-workers previously noted that 2D ^{1}H–^{13}C CP-HETCOR spectra of piroxicam HCl obtained with FSLG homonuclear decoupling possessed tilted cross-peaks, likely due to correlated susceptibility broadening.[14] More recently, Mali and co-workers applied 2D ^{1}H–^{13}C HETCOR solid-state NMR experiments without homonuclear decoupling to reduce a substantial ABMS broadening on the order of 3 ppm observed within a MOF containing aromatic linkers.[13] The observation of tilted cross-peaks and enhanced resolution in the HETCOR spectrum proved that the peak broadening was due to ABMS rather than structural disorder.[13]

Here we demonstrate that 2D ^{1}H–^{13}C CP-HETCOR experiments in combination with modern homonuclear decoupling schemes can be generally applied to reduce inhomogeneous ABMS broadening on the order of 1 ppm typically encountered in organic solids and APIs with aromatic groups. For samples with significant ABMS broadening the ^{1}H and ^{13}C solid-state NMR spectra extracted from the 2D HETCOR spectrum have resolution that is superior to that observed from the corresponding 1D NMR spectra of the sample diluted in a material with isotropic susceptibility. Systematic comparisons of 1D solid-state NMR spectra and ^{1}H and ^{13}C solid-state NMR spectra obtained from a 2D ^{1}H–^{13}C HETCOR NMR spectrum shows that the HETCOR spectrum may directly increase spectral resolution by factors of 1.5 to 8 under applied magnetic fields of 9.4 T to 18.8 T. 2D ^{1}H–^{13}C CP-HETCOR experiments are advantageous for reducing ABMS broadening because they are frequently performed with natural abundance of ^{13}C and provide high resolution ^{1}H solid-state NMR spectra. The main

limitation on resolution in the HETCOR spectrum is likely the homogeneous proton linewidth under homonuclear decoupling. However, because the homogeneous proton linewidth is typically field independent and inhomogeneous ABMS broadening scales with applied field, 2D ^{1}H–^{13}C HETCOR experiments can provide large gains in resolution under high magnetic fields. 2D ^{1}H–^{13}C CP-HETCOR experiments are then applied to resolve the ^{1}H and ^{13}C NMR signals of a mixture of two polymorphic forms of aspirin.

Results and discussion

2D ^{1}H–^{13}C HETCOR experiments on hexamethylbenzene

First we apply 2D ^{1}H–^{13}C CP-HETCOR solid-state NMR experiments to hexamethylbenzene (HMB) because it is well known that the ^{1}H and ^{13}C solid-state NMR spectra of HMB display substantial ABMS broadening,[5,6,12] and it is a commonly used "setup sample" in many labs. Fig. 1 shows 2D ^{1}H–^{13}C CP-HETCOR spectra of HMB acquired at 9.4 T and 18.8 T. eDUMBO-1_{22} homonuclear decoupling[40] was applied during the ^{1}H indirect dimension evolution time (t_1) of the 2D HETCOR experiments. Homonuclear decoupling is critical to reduce the homogeneous linewidths of the ^{1}H peaks and obtain high resolution HETCOR spectra. The ^{13}C NMR spectra of HMB give peaks with FWHM of ~1.0 ppm in the projections of the ^{13}C dimension under both magnetic fields. Under both magnetic fields, the ^{1}H NMR peaks of the methyl groups in the projections of the 2D ^{1}H–^{13}C HETCOR spectra also have FWHM of ~1 ppm. A 1D ^{13}C CPMAS spectrum of HMB diluted in potassium bromide (~10% HMB by volume) was also obtained to illustrate the effects on resolution of diluting HMB in a matrix with isotropic susceptibility (Fig. S1, ESI†). This diluted sample gives a ^{13}C peak FWHM of 0.75 ppm, which represents about a factor of 1.5 improvement in resolution compared to a 1D ^{13}C solid-state NMR spectrum of pure HMB. The improvement in resolution upon dilution is consistent with previously reported solid-state NMR experiments on diluted samples.[5,7] The similarity of the FWHM of the ^{1}H and ^{13}C peaks in the HETCOR projections and the reduction in FWHM upon dilution in KBr confirm that ABMS is the primary broadening mechanism in HMB.

Inspection of the 2D ^{1}H–^{13}C HETCOR spectra of HMB shows that they possess tilted cross-peaks. The tilted cross-peaks arise because the peak positions of the correlated ^{1}H and ^{13}C spins will be shifted by the same amount in ppm due to the ABMS broadening.[13,18] In order to quantify the direct gain in resolution provided by the HETCOR spectrum we extracted the individual rows and columns of the 2D ^{1}H–^{13}C HETCOR spectrum and compared them with the corresponding projections.[18] For example, at 9.4 T the methyl peak in the ^{13}C NMR spectrum obtained from a single row of the 2D spectrum has a FWHM of 0.31 ppm, while the FWHM of the methyl ^{13}C NMR peak is 1.12 ppm in the projection of the 2D spectrum (this is the same resolution observed in a 1D CPMAS spectrum). Similarly, the ^{1}H NMR spectrum obtained from a single column of the 2D spectrum has a FWHM of 0.28 ppm, while the projection of the ^{1}H dimension gives a FWHM of 1.13 ppm. Therefore, by reducing the ABMS broadening there is more than a factor of 3.6 direct improvement in the resolution of the ^{1}H and ^{13}C NMR spectra obtained from the 2D HETCOR spectrum as compared to the corresponding NMR spectra obtained from the projections. The ^{13}C NMR spectrum obtained from a row of the 2D HETCOR spectrum also has more than 2 times better resolution than a 1D ^{13}C CPMAS spectrum of a diluted sample (Fig. S1, ESI†). As an alternative to extracting individual slices from the 2D HETCOR spectrum, a shearing transformation could be applied to obtain ^{1}H and ^{13}C projections with improved spectral resolution

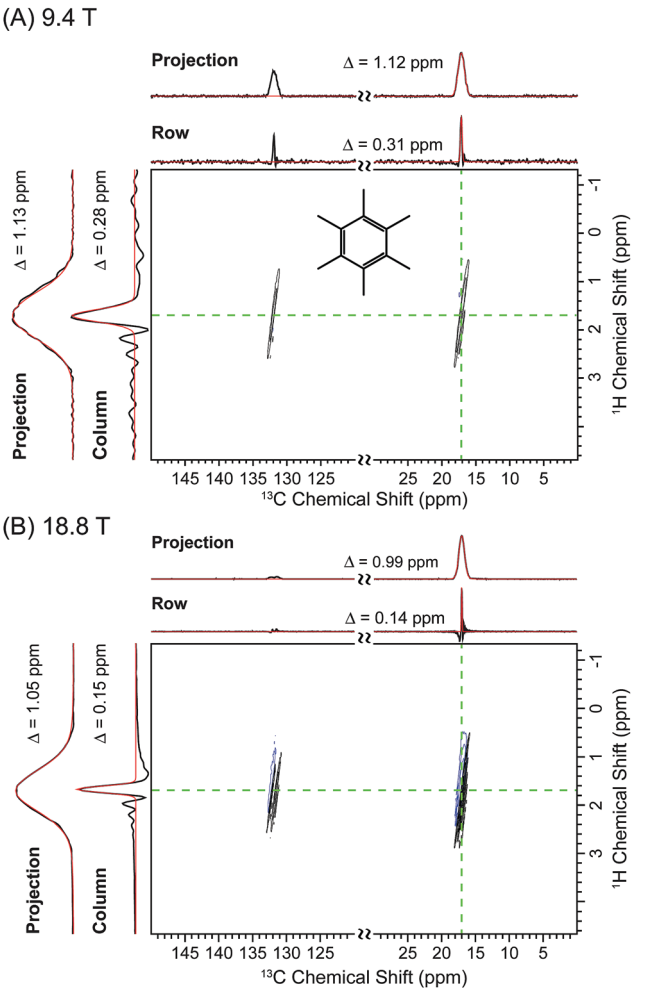

Fig. 1 2D ^{1}H–^{13}C dipolar HETCOR solid-state NMR spectra of hexamethylbenzene (HMB) acquired with eDUMBO-1_{22} ^{1}H homonuclear decoupling applied during the t_1 evolution period. Spectra were acquired with external magnetic fields of (A) 9.4 T (23 minutes experimental time) and (B) 18.8 T (1.1 hours experimental time). The MAS frequency was ν_r = 8928 Hz in both cases. The positive projections of the 2D spectrum are compared to individual rows and columns of the 2D experiments. The red lines overlaid on the projections and rows/columns are fits of the methyl peaks to a mixed Lorentzian/Gaussian function. The FWHM (Δ) determined from the fit is indicated. The dashed green lines indicate the rows and columns used for resolution comparisons. Due to the reduction of ABMS broadening, the rows/columns have 3.6 and 7.1 times higher resolution than the corresponding projections for the 9.4 T and 18.8 T spectra, respectively.

(Fig. S2, ESI†). However, in samples with many peaks, single rows/columns of the 2D spectrum will likely give sub-spectra with better resolution since the homogeneous ^{1}H linewidths will vary for different peaks in the spectrum (*vide infra*). More advanced deconvolution methods may also be applied to obtain a 2D spectrum with improved resolution.[41,42]

Importantly, a 2D HETCOR spectrum enables improved resolution to be realized under higher applied magnetic fields. Note that 1D ^{13}C CPMAS or 1D ^{1}H stroboscopic CRAMPS solid-state NMR spectra of HMB will not show improved resolution under higher magnetic fields because the inhomogeneous ABMS broadening scales with the applied field. In the 18.8 T 2D ^{1}H–^{13}C CP-HETCOR spectrum of HMB, the ^{1}H and ^{13}C peaks in the projections of the 2D spectrum once again show FWHM of ~1 ppm because of the inhomogeneous ABMS broadening. The ^{1}H and ^{13}C NMR spectra extracted from slices of the 2D HETCOR spectrum acquired at 18.8 T now yield ^{1}H and ^{13}C NMR spectra with FWHM of the methyl peaks of only ~0.15 ppm. Comparison of the slices and projections illustrates that the 2D HETCOR spectrum provides a factor of 7 direct improvement in resolution. These dramatic gains in resolution are possible because HMB has a constant and field independent ^{1}H homogeneous linewidth of ~115 Hz under the application of ^{1}H homonuclear decoupling. The small ^{1}H homogeneous linewidth in HMB likely arises because the homonuclear ^{1}H dipolar couplings are partially averaged both by rapid jumps/rotations of the HMB molecules about their six-fold rotational axis and by the rotation of the methyl groups about their three-fold rotational axis.

In summary, the experiments on HMB at 9.4 T and 18.8 T illustrate that the direct gain in resolution provided by 2D HETCOR experiments is given by the ratio of the inhomogeneous ABMS ^{13}C/^{1}H linewidth to the homogeneous ^{1}H linewidth ($\Delta_{\text{inhom. ABMS}}/\Delta_{\text{hom.}}$), with the former determined by the magnitude of the ABMS broadening and the strength of the applied field and the latter determined by the efficiency of the homonuclear decoupling. This is why the FWHM measured in ppm in the slices from the 18.8 T 2D HETCOR spectrum are about half of those measured in the slices from the 9.4 T 2D HETCOR spectrum. In rigid organic solids, the homogeneous ^{1}H linewidth (Δ_{hom}) will likely be the factor that limits the resolution in the slices obtained from the 2D HETCOR spectrum (*vide infra*).

DNP enhanced 2D ^{1}H–^{13}C HETCOR experiments on salicylic acid

Fig. 2A shows a 9.4 T DNP enhanced 2D ^{1}H–^{13}C HETCOR spectrum of finely ground crystalline salicylic acid. DNP was applied to enhance NMR sensitivity because salicylic acid has long proton longitudinal relaxation times (T_1), which were estimated to be longer than 60 s at room temperature. The relayed spin diffusion DNP method[43–46] was used to enhance the sensitivity of solid-state NMR experiments on salicylic acid. To prepare the salicylic acid for DNP experiments it was ground by hand with a mortar and pestle into a fine powder. The powder was then impregnated with a 16 mM solution of the DNP polarizing agent TEKPol[47] dissolved in 1,1,2,2-tetrachloroethane (TCE).[48] Salicylic acid is insoluble in the TCE-biradical solution; therefore, the ^{1}H nuclei in the interior of the salicylic acid crystallites are polarized by transport of DNP enhanced ^{1}H polarization from the surface of the particles by proton spin diffusion.[43,44,46] The ^{1}H–^{13}C CPMAS DNP signal enhancement ($\varepsilon_{\text{C CP}}$) was estimated to be larger than a factor of 75 for salicylic acid. The long proton T_1 of salicylic acid at cryogenic temperatures enables high DNP enhancement to be obtained.[43,44]

For salicylic acid all of the ^{13}C peaks have FWHM of *ca.* 1.2 ppm in the ^{13}C projection obtained from the 2D ^{1}H–^{13}C HETCOR spectrum. The projection of the homonuclear

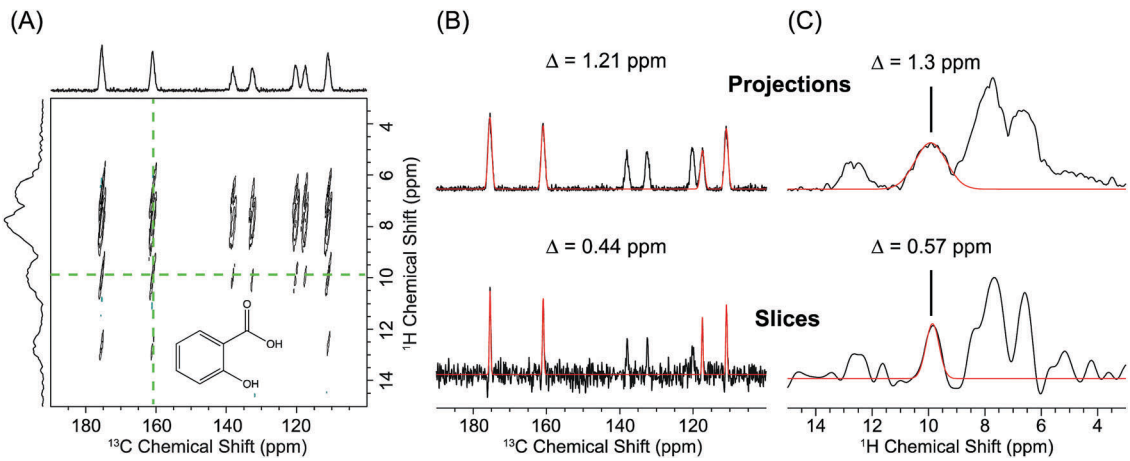

Fig. 2 (A) 9.4 T DNP enhanced 2D ^{1}H–^{13}C dipolar HETCOR solid-state NMR spectrum of salicylic acid. The spectrum was acquired with eDUMBO-1_{22} ^{1}H homonuclear decoupling applied during the t_1 evolution period and a 2.5 ms CP contact time. The MAS frequency was ν_r = 8000 Hz. (B and C) The positive ^{13}C and ^{1}H projections of the 2D spectrum are compared to the ^{13}C and ^{1}H NMR spectra obtained from the individual rows and columns of the 2D spectrum. The red lines overlaid on the projections and slices are fits of the peaks to a mixed Lorentzian/Gaussian function. The average FWHM (Δ) determined from the fit is indicated. The dashed green lines indicate the rows and columns used for resolution comparisons. The ^{13}C and ^{1}H NMR spectra from the slices have 2.7 and 2.3 times higher resolution than the corresponding projections, respectively.

decoupled ^{1}H indirect dimension displays peaks with FWHM of $\sim$1.3 ppm which are similar to FWHM observed for ^{13}C (Fig. 2C). The similar FWHM of the ^{1}H and ^{13}C peaks confirm that ABMS is the primary inhomogeneous broadening mechanism. Once again, if single rows/columns of the 2D HETCOR spectrum are extracted then there is a dramatic improvement in the resolution of the ^{13}C/^{1}H NMR spectra. In the slices the FWHM is reduced to $\sim$0.44 and 0.56 ppm for ^{13}C and ^{1}H peaks, respectively (see Table S1, ESI,† for a detailed summary of ^{13}C FWHM). This corresponds to a factor of 2.7 and 2.3 improvement in resolution in comparison to the ^{13}C and ^{1}H NMR spectra obtained from projections. Note that a relatively long contact time of 2.5 ms was used for the ^{1}H–^{13}C CP step in the 2D HETCOR experimental time. Homonuclear ^{1}H spin diffusion during the 2.5 ms CP contact pulse causes relayed polarization transfers and produces correlations between the hydroxyl proton at 9.8 ppm ^{1}H chemical shift and all of the ^{13}C resonances. This single row yields a high resolution ^{13}C NMR spectrum which contains all peaks in the sample. If instead a row centered on the aromatic protons at 7.8 ppm ^{1}H chemical shift is used, then the FWHM of the ^{13}C peaks are around 0.8 ppm (Fig. S3 and Table S1, ESI†). This is because the aromatic protons have a larger homogeneous ^{1}H linewidth and there is also likely partial overlap of aromatic ^{1}H signals with distinct isotropic chemical shifts. Both of these mechanisms will reduce the resolution of the individual rows/columns and the 2D HETCOR plot. This also highlights a limitation of using the 2D HETCOR spectrum to remove ABMS and increase resolution; if a long contact time HETCOR experiment is used to obtain a single row with all ^{13}C peaks, then the ^{1}H signal that is used to obtain the ^{13}C NMR spectrum should not overlap with any other ^{1}H NMR signals. This may be challenging in complex molecules with many ^{1}H NMR signals. Alternatively, selective 2D HETCOR spectra could be obtained with shorter contact times to provide an additional gain in resolution/dispersion, minimize ^{1}H peak overlap and resolve overlapping ^{13}C signals either in individual rows or on the 2D HETCOR plot. However, with short contact times it is impossible to obtain a single row/column with all of the ^{13}C/^{1}H signals.

For salicylic acid the FWHM of the ^{1}H and ^{13}C peaks are around 0.5 ppm in the slices extracted from the 2D HETCOR spectrum. This is significantly lower resolution than was observed for HMB where ^{1}H and ^{13}C peaks with FWHM around 0.15 ppm were observed in the slices of the HETCOR spectrum. The increase in FWHM for salicylic acid as compared to HMB occurs because the homogeneous linewidth of the ^{1}H peaks in the slices of the 2D HETCOR spectrum determines the resolution (in ppm) in both the ^{1}H and ^{13}C dimensions. As discussed above, there is substantial motional/dynamic averaging of the ^{1}H homonuclear dipolar couplings in HMB. However, salicylic acid is a rigid crystalline solid; therefore, the increase in homogeneous ^{1}H linewidths probably reflects stronger homonuclear ^{1}H dipolar couplings in salicylic acid as compared to HMB. Highly optimized modern ^{1}H CRAMPS solid-state NMR spectra typically give ^{1}H peaks with homogeneous linewidths around 200 Hz in rigid crystalline organic solids (0.5 ppm at 9.4 T).[40,49–52]

DNP enhanced solid-state NMR experiments on salicylic acid diluted in lactose

DNP enhanced solid-state NMR experiments were also performed on salicylic acid diluted in lactose to determine if 2D HETCOR experiments on pure salicylic acid or a 1D ^{13}C CPMAS experiment on the diluted sample provides better resolution and sensitivity. Salicylic acid was approximately 10% of the volume of the solid material in the diluted sample. For diluted salicylic acid the average FWHM of the ^{13}C peaks in a 1D CPMAS spectrum was 0.65 ppm (Fig. 2B), which represents nearly a two-fold improvement in spectral resolution as compared to the pure salicylic acid sample (average ^{13}C peak FWHM of 1.21 ppm). We note that the 1D ^{13}C CPMAS spectrum of the 10% diluted sample could be obtained in a shorter experimental time than the 2D HETCOR spectrum of the pure sample. The absolute sensitivity was more than five times higher for 1D ^{13}C CPMAS experiments on the diluted salicylic acid sample as compared to the 2D HETCOR experiments on the pure salicylic acid (Fig. S3, ESI†). The reduced sensitivity for the HETCOR experiment occurs because non-optimal recycle delays were used to reduce the experimental time of the HETCOR experiment and 2D acquisition normally results in a significant sensitivity loss due to signal decay in the indirect dimension. However, with the high sensitivity provided by DNP it was possible to obtain a high quality 2D ^{1}H–^{13}C CP-HETCOR spectrum of the diluted salicylic acid sample in $\sim$4.5 hours (Fig. S4, ESI†). The ^{13}C NMR spectra extracted from the rows of the 2D HETCOR spectrum gave an average ^{13}C peak FWHM of 0.37 ppm, which represents a factor of 1.8 direct improvement in resolution compared to the 1D ^{13}C CPMAS spectrum of the diluted sample. In comparison, the ^{13}C NMR spectra extracted from the rows of the 2D HETCOR spectrum of pure salicylic acid gave an average ^{13}C FWHM of 0.44 ppm (Fig. 2B).

In summary, the experiments on hexamethylbenzene, salicylic acid and aspirin suggest that 2D ^{1}H–^{13}C HETCOR experiments have a sensitivity that is about 5–7 times lower than that of the corresponding 1D CPMAS experiment. In cases where sensitivity is a limitation, dilution could be the preferred method to reduce ABMS broadening as it may provide up to a 2-fold improvement in resolution, consistent with previous experiments on diluted materials.[5,7] However, the 2D HETCOR spectrum simultaneously provides ^{13}C NMR spectra with the highest direct resolution and provides additional information and resolution by correlating the ^{13}C chemical shifts with the high resolution ^{1}H NMR spectra. The resolution of the HETCOR NMR spectra will also improve under a higher magnetic field, while the resolution of a 1D solid-state NMR spectrum of a diluted sample will remain constant.

Solid-state NMR experiments on dicoumarol and ibuprofen

In order to test the general applicability of 2D HETCOR NMR experiments to reduce broadening due to ABMS, we also performed experiments on dicoumarol and ibuprofen. Ground dicoumarol exhibited very broad peaks at 9.4 T and 105 K, suggesting that ABMS broadening was substantial (FWHM $\approx$ 1.7 ppm in the ^{13}C projection of the DNP enhanced 2D ^{1}H–^{13}C CP-HETCOR

spectrum). A row extracted from a DNP enhanced 2D ^{1}H–^{13}C HETCOR spectrum of dicoumarol gave a ^{13}C NMR spectrum with ~1.4 times higher resolution (Fig. S5 and Table S2, ESI†). For ibuprofen we observed an average FWHM of less than 0.45 ppm for the ^{13}C peaks in the 1D ^{1}H–^{13}C CPMAS spectrum obtained at 18.8 T (Fig. S6 and Table S3, ESI†). This suggests that the inhomogeneous broadening due to ABMS is small for ibuprofen, consistent with previous reports.[7] Consequently, the average FWHM of the ^{13}C peaks is around 0.39 ppm in the row extracted from the 2D ^{1}H–^{13}C HETCOR spectrum and there is only a modest improvement in resolution. Below we describe how 2D ^{1}H–^{13}C HETCOR experiments can be applied to detect different polymorphs in lyophilized aspirin.

Observing polymorphs of aspirin using 2D ^{1}H–^{13}C HETCOR experiments

Acetylsalicylic acid (aspirin) is one of the oldest and most widely consumed pharmaceuticals. The crystal structure of the most common form of aspirin (form I) was initially solved in 1964.[53] However, on the basis of melting point and dissolution rate measurements it had long been hypothesized that a second crystalline form of aspirin (form II) existed.[54–56] In 2004 Ouvrard and Price predicted the existence of aspirin form II using crystal structure prediction calculations and suggested that the energies of form I and form II are essentially identical.[57] In 2005 Munson and co-workers reported that a lyophilized sample of aspirin showed a second methyl ^{13}C peak in its ^{13}C CPMAS solid-state NMR spectrum and hypothesized that this second peak corresponded to a different crystalline form of aspirin.[58] Zaworotko and co-workers subsequently presented a crystal structure of form II in 2005; however, the structure they reported showed large *R*-factors.[59] Bond *et al.* then confirmed the proposed crystal structure of form II by performing X-ray diffraction on higher purity single crystals.[60] They also showed that because forms I and II have very similar structures, it is likely that form I and form II exist as inter-grown crystals[61] and this explained why the isolation and crystal structure determination of form II crystals were challenging.[60] Bond *et al.* recently managed to produce diffraction quality single crystals of higher purity form II by crystallizing aspirin in the presence of aspirin anhydride.[56] Very recently, a third stable form of aspirin, form IV, was successfully crystallized from molten aspirin.[62]

Fig. 3 shows the 1D ^{1}H–^{13}C CPMAS and 2D ^{1}H–^{13}C HETCOR solid-state NMR spectra of lyophilized aspirin obtained with a magnetic field of 18.8 T. The methyl region of the 1D ^{1}H–^{13}C CPMAS spectrum of lyophilized aspirin appears to contain two overlapping ^{13}C NMR signals in the methyl region (Fig. 3B). There is an intense methyl ^{13}C NMR signal with an isotropic chemical shift of 20.0 ppm, which matches the chemical shift previously reported for the methyl group in form I of aspirin.[63,64] The second methyl ^{13}C NMR signal appears as a low intensity shoulder on the main peak and has a chemical shift of 20.7 ppm, which we assign to aspirin form II (*vide infra*). However, the peaks in the 1D ^{1}H–^{13}C CPMAS spectrum have FWHM of ~0.7 ppm and low resolution prevents the overlapping methyl signals from being clearly resolved. A 1D ^{13}C CPMAS

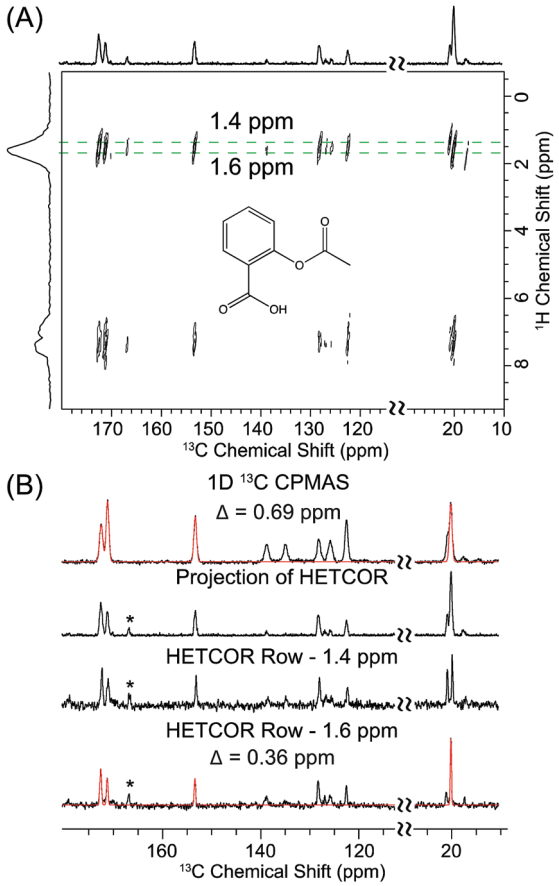

Fig. 3 (A) 18.8 T 2D ^{1}H–^{13}C CP-HETCOR solid-state NMR spectrum of lyophilized aspirin. The spectrum was acquired with eDUMBO-1_{22} ^{1}H homonuclear decoupling applied during the t_1 evolution period and a 2.5 ms CP contact time. The MAS frequency was ν_r = 8928 Hz. (B) Comparison of ^{13}C solid-state NMR spectra of lyophilized aspirin obtained using a 1D ^{1}H–^{13}C CPMAS experiment and ν_r = 12 500 Hz (top trace), the projection of the 2D HETCOR spectrum, and spectra extracted from the rows of the HETCOR spectrum at ^{1}H chemical shifts of 1.40 ppm and 1.65 ppm (lower trace). The red lines overlaid on the spectra are fits of the resolved peaks to a mixed Lorentzian/Gaussian function. The average FWHM (Δ) determined from the fits is indicated. The dashed green lines indicate the rows used for resolution comparisons.

spectrum of 14 volume% lyophilized aspirin diluted in KBr was also obtained. In the diluted sample the average FWHM of the ^{13}C peaks was 0.6 ppm and this corresponds to a marginal improvement in resolution as compared to the 1D ^{13}C CPMAS spectrum of pure material (Fig. S7, ESI†).

A 2D ^{1}H–^{13}C HETCOR spectrum of lyophilized aspirin was obtained at 18.8 T to determine if distinct ^{1}H and ^{13}C chemical shifts could be observed for form I and form II. The 2D ^{1}H–^{13}C HETCOR spectrum clearly shows tilted cross-peaks which are characteristic of ABMS broadening being the dominant contribution to the inhomogeneous linewidth. Comparison of the 1D ^{1}H–^{13}C CPMAS and 2D HETCOR spectra illustrates significant improvement in resolution in the rows/columns of the 2D HETCOR spectrum. The ^{13}C peaks in the rows extracted from the HETCOR spectrum have an average FWHM of 0.36 ppm, while an average FWHM of 0.69 ppm was observed in the

1D ^{1}H–^{13}C CPMAS spectrum (FWHM are summarized in Table S4, ESI†). Therefore, the 2D HETCOR spectrum provides nearly a two-fold improvement in direct resolution. The added dispersion from the ^{1}H dimension in the 2D HETCOR spectrum also helps in separating and resolving overlapping signals.

The chemical shifts of the methyl groups associated with form I [$\delta_{iso}(^{13}C)$ = 20.0 ppm, $\delta_{iso}(^{1}H)$ = 1.6 ppm] and form II [$\delta_{iso}(^{13}C)$ = 20.7 ppm, $\delta_{iso}(^{1}H)$ = 1.4 ppm] can be directly read from the 2D HETCOR spectrum or from the individual columns/rows (Fig. 3B and Fig. S8, ESI†). Comparison of the ^{13}C solid-state NMR spectra obtained from the rows of the HETCOR spectrum at these two ^{1}H chemical shift positions suggests that the methyl ^{13}C NMR peaks are the only ones which have substantially different isotropic chemical shifts in form I and form II. Plane-wave DFT GIPAW calculations of ^{1}H and ^{13}C chemical shifts for form I and form II are consistent with the experimental results and predict the largest ^{1}H and ^{13}C chemical shift differences for the methyl groups (Tables S5 and S6, ESI†). The known single crystal X-ray diffraction structures of form I and form II show that the main difference in the two crystal structures is the relative orientations of the methyl groups of adjacent aspirin molecules within the lattice,[59,60] and this likely explains why the methyl carbons and hydrogen of each form show the largest ^{13}C and ^{1}H isotropic chemical shift differences.

The DFT calculations also predict that there is a difference in the calculated isotropic ^{13}C chemical shifts for the protonated aromatic carbon that is ortho to the acetyl group (C3, Fig. S9, ESI†). However, it is difficult to determine the experimental ^{13}C chemical shift values for C3 in form I and form II because these resonances are of low intensity at 18.8 T due to substantial chemical shift anisotropy. The form II signals are also obscured by the much more intense form I signals. Subsequently, DNP enhanced 9.4 T 1D ^{1}H–^{13}C CPMAS and 2D ^{1}H–^{13}C HETCOR solid-state NMR spectra of lyophilized aspirin were obtained to see if the ortho carbon signals of the two forms could be resolved with better sensitivity provided by DNP (Fig. S10, ESI†). The DNP enhancement for both forms was identical ($\varepsilon_{C\,CP}$ = 7.5), which is consistent with the fact that both forms are likely inter-grown and present within the same crystallites.[61] Note that the ^{1}H and ^{13}C chemical shifts slightly differ in the 105 K DNP enhanced and conventional room temperature solid-state NMR spectra. For example, the chemical shifts of the methyl groups associated with form I [$\delta_{iso}(^{13}C)$ = 19.8 ppm, $\delta_{iso}(^{1}H)$ = 1.6 ppm] and form II [$\delta_{iso}(^{13}C)$ = 20.9 ppm, $\delta_{iso}(^{1}H)$ = 1.2 ppm] differ from those at room temperature. The low sample temperature and lower magnetic field of 9.4 T used for acquisition of the DNP enhanced 2D ^{1}H–^{13}C HETCOR experiment leads to slightly poorer resolution as compared to the solid-state NMR spectra obtained under the higher field of 18.8 T. However, examination of the ^{13}C peak assigned to the carbon ortho to the acetyl group in form I shows that there is a primary intense signal at $\delta_{iso}(^{13}C)$ = 125.1 ppm and a weak shoulder at a slightly higher chemical shift of $\delta_{iso}(^{13}C)$ = 125.4 ppm which is assigned to the C3 signal of form II.

Conclusions

Here we have shown that when ABMS is the dominant inhomogeneous broadening mechanism 2D HETCOR NMR spectra can provide direct gains in spectral resolution of a factor of 1.5 to 8 as compared to the corresponding 1D spectrum. The direct gain in resolution achieved in the rows/columns of the 2D HETCOR spectrum depends on the ratio of the inhomogeneous ^{13}C/^{1}H linewidth due to ABMS to the homogeneous ^{1}H linewidth ($\Delta_{inhom.\ ABMS}/\Delta_{hom.}$). Higher magnetic fields lead to larger inhomogeneous ABMS broadening, which enables the 2D ^{1}H–^{13}C HETCOR experiments to further enhance resolution. Modern homonuclear decoupling schemes such as eDUMBO-1_{22}, PMLG, LG-4, TIMES, *etc.*, typically result in homogeneous ^{1}H linewidths of around 200 Hz ($\sim$0.5 ppm at 9.4 T).[40,49–52] A homogeneous ^{1}H linewidth of 200 Hz would correspond to 2D HETCOR slices with ^{1}H and ^{13}C NMR spectra with peaks with FWHM of 0.5 ppm at 9.4 T and 0.25 ppm at 18.8 T. Therefore, in order for the 2D ^{1}H–^{13}C HETCOR approach to be able to improve resolution, the inhomogeneous broadening due to ABMS likely must be greater than 0.5 ppm. Note that the refocused ^{13}C transverse relaxation time (T_2') of rigid protonated organic solids is usually longer than 20 ms and this corresponds to a homogeneous ^{13}C linewidth of less than 15 Hz.[65,66] Therefore, the homogeneous ^{13}C linewidth is unlikely to make a substantial contribution to the observed linewidth in the slices of the 2D HETCOR spectra. For the samples studied here the 2D HETCOR spectra provided better direct resolution than 1D solid-state NMR spectra of samples diluted in materials with isotropic susceptibility.

We anticipate that the 2D HETCOR strategy outlined here represents a simple and highly sensitive method to improve the resolution of ^{1}H and ^{13}C solid-state NMR spectra of aromatic organic solids with next generation high field NMR spectrometers which have magnetic fields above 35 T.[67] 2D HETCOR solid-state NMR experiments under higher applied magnetic fields will also bring other well known benefits such as improved ^{1}H NMR signal dispersion. Our results also suggest that 2D HETCOR experiments could be useful for the final optimization and testing of homonuclear and heteronuclear decoupling schemes under high magnetic fields where the limiting factor on resolution is likely to be inhomogeneous ABMS broadening.

Experimental

Hexamethylbenzene, dicoumarol, salicylic acid, ibuprofen, lactose and potassium bromide were purchased from Sigma Aldrich and used without further purification. Aspirin was purchased from Fluka. Samples of aspirin containing both form I and form II were prepared by lyophilizing a 1 mg mL^{-1} solution of aspirin in deionized water. Vials containing 5 mL of the solution were lyophilized with a VirTis AdVantage Plus benchtop freeze dryer. The solution was cooled to -5 °C and held at this temperature for 30 minutes, and then cooled and held at -45 °C for two hours. The frozen solution was then warmed to -35 °C and the primary drying step was performed

by subjecting the sample to a 60 mTorr vacuum for 72 hours at this temperature. The sample was then warmed to 30 °C over the course of 8 hours and held at this temperature for 4 additional hours to remove any remaining water.

In order to prepare samples of dicoumarol and salicylic acid for relayed DNP experiments they were finely ground by hand in a mortar and pestle for several minutes in order to reduce the particle sizes.[44] The lyophilized aspirin sample was not ground in order to avoid inducing phase transitions between the two polymorphic forms. The powdered solids were then impregnated[68] with a 16 mM solution of TEKPol[47] in 1,1,2,2-tetrachloroethane[48] (salicylic acid), an 11 mM solution of AMUPol[69] in glycerol-d_8/D_2O/H_2O 60/30/10 (dicoumarol), or a 16 mM solution of TEKPol in 1,3-dibromobutane (lyophilized aspirin). The impregnated samples were then packed into 3.2 mm sapphire rotors and capped with PTFE inserts.

In order to demonstrate the effects of sample dilution on ABMS broadening, solid-state NMR experiments were performed on samples of hexamethylbenzene, salicylic acid and lyophilized aspirin diluted in solids with isotropic susceptibility or negligible ABMS (KBr and lactose). 4.0 mg of hexamethylbenzene was mixed in 96 mg of KBr to give a solid mixture which was ~10% hexamethylbenzene by volume. 10.2 mg of finely ground salicylic acid was mixed with 90.1 mg of ground lactose to give a solid mixture which was ~10% salicylic acid by volume. 35 mg of the lactose/salicylic acid mixed powder was then impregnated with 20 mL of 16 mM TEKPol[47] 1,1,2,2-tetrachloroethane solution and transferred to a sapphire DNP rotor. 7.9 mg of finely ground lyophilized aspirin was mixed with 91.9 mg of KBr to give a mixture which was ~14% aspirin by volume.

Conventional solid-state NMR experiments were performed on a standard bore 18.8 T spectrometer or a wide bore 9.4 T spectrometer, both of which were equipped with a Bruker Avance III HD console. A Bruker 3.2 mm triple resonance HCN probe was used for acquisition of all spectra at 18.8 T. A 2.5 mm HXY triple resonance probe was used for conventional solid-state NMR experiments at 9.4 T. DNP enhanced solid-state NMR experiments were performed on a Bruker 9.4 T 400 MHz/263 GHz solid-state NMR spectrometer[70] equipped with a Bruker Avance III console. A Bruker 3.2 mm triple resonance DNP probe configured in HCN triple resonance mode was used for acquisition of all spectra. The sample temperature for DNP experiments was approximately 110 K. Adamantane and labelled glycine-2-^{13}C-^{15}N were used to optimize CP experiments and homonuclear decoupling conditions. ^{1}H pulse lengths and rf fields were directly calibrated on the samples of interest. The ^{1}H chemical shifts were referenced to neat tetramethylsilane by using adamantane ($\delta_{iso}(^1H)$ = 1.82 ppm) as a secondary chemical shift standard. ^{13}C chemical shifts were referenced to neat tetramethylsilane by use of adamantane ($\delta_{iso}(^{13}C)$ = 38.48 ppm). For the samples on which HETCOR experiments were performed the sample was confined to the central half of the rotor to reduce rf inhomogeneity. This was done by packing powdered polytetrafluoroethylene or KBr below and above the sample of interest into the upper and lower quarters of the rotor.

All CPMAS experiments[71,72] were performed with a variable amplitude ^{1}H contact pulse which was linearly ramped from a 90% to 100% rf field to broaden the Hartmann–Hahn match conditions.[73] The rf field of the spin lock pulses in the CP experiments was typically between 50 and 75 kHz for ^{1}H and ^{13}C. SPINAL-64 ^{1}H heteronuclear decoupling was applied during ^{13}C signal acquisition with a ^{1}H rf field of 100 kHz.[74] The ^{13}C signal acquisition time was between 30 and 40 ms in all cases. The pulse sequence used for acquisition of 2D ^{1}H–^{13}C CP-HETCOR solid-state NMR spectra is shown in Fig. S11 (ESI†).[75,76] eDUMBO-1_{22} homonuclear ^{1}H decoupling[40] was applied during the indirect dimension evolution period (t_1). The eDUMBO-1_{22} pulse duration and rf field was 40.0 μs and 96 kHz, respectively, for HETCOR experiments at 18.8 T. The eDUMBO-1_{22} pulse duration and rf field was 32.0 μs and 100 kHz, respectively, for DNP enhanced HETCOR experiments at 9.4 T. The ^{1}H spectral width was scaled by a factor of 1.7 to 1.9 to correct for scaling of the ^{1}H chemical shift by homonuclear decoupling. The total indirect dimension evolution time in the ^{1}H–^{13}C HETCOR experiments was typically longer than 6 ms. The MAS frequency for all HETCOR experiments was between 7500 and 9000 Hz. DNP enhanced HETCOR spectra were typically acquired with 2 to 16 scans per increment, while conventional HETCOR spectra required 4 to 32 scans per increment. Shifted Gaussian apodization functions were applied to the ^{1}H and ^{13}C NMR spectra in order to improve resolution and these parameters are reported in Table S7 (ESI†).

Plane-wave DFT calculations were performed with CASTEP[77] within the Materials Studio software package. All calculations used the Perdew–Burke–Ernzerhof (PBE) exchange correlation functional[78] with ultrasoft pseudopotentials generated on-the-fly.[79] The calculations used a plane-wave basis set with a maximum cutoff energy of 800 eV, with integrals taken over the Brillouin zone by using a Monkhorst–Pack grid with a minimum sample spacing of 0.09 Å. ^{1}H and ^{13}C chemical shieldings were calculated using the GIPAW method.[80] Calculated ^{13}C chemical shifts were derived using a reference shielding value obtained through linear regression of a plot of calculated shielding *vs.* experimental shifts (see the ESI† for details). The room temperature crystal structures of aspirin form I (CSD code: ACSALA07)[81] and form II (CSD code: ACSALA17)[61] were used for calculations. Prior to the calculation of chemical shielding, the hydrogen atom positions were optimized, while the unit cell parameters and heavy atom positions were fixed. The calculated chemical shielding values and chemical shifts are reported in Tables S5 and S6 (ESI†).

Conflicts of interest

The authors declare the following competing financial interest(s): E. J. M. is a partial owner of Kansas Analytical Services, a company that provides solid-state NMR services to the pharmaceutical industry. The results presented here are from academic work at the University of Kentucky, and no data from Kansas Analytical Services are presented.

Acknowledgements

This material is based upon work supported by the National Science Foundation under Grant No. 1709972 (AJR) and 1710453 (EJM). This work was supported in part by the NSF I/UCRC Center for Pharmaceutical Development (IIP-1063879, 1540011, and industrial contributions). AJR thanks Iowa State University and the Ames Laboratory (Royalty Account) for additional support. The Ames Laboratory is operated for the U.S. DOE by Iowa State University under contract no. DE-AC02-07CH11358. We thank Dr Gilles Casano, Dr Olivier Ouari and Prof. Paul Tordo (Aix-Marseille University) for providing the AMUPol and TEKPol biradicals. We thank Dr Bruce Fulton (Iowa State University) for assistance with 800 MHz solid-state NMR experiments.

References

1 J. Bernstein, *Polymorphism in Molecular Crystals*, Oxford University Press, Oxford, 2002.
2 R. T. Berendt, D. M. Sperger, P. K. Isbester and E. J. Munson, *TrAC, Trends Anal. Chem.*, 2006, **25**, 977–984.
3 R. K. Harris, *Analyst*, 2006, **131**, 351–373.
4 F. G. Vogt, *Future Med. Chem.*, 2010, **2**, 915–921.
5 D. L. Vanderhart, W. L. Earl and A. N. Garroway, *J. Magn. Reson.*, 1981, **44**, 361–401.
6 M. Alla and E. Lippmaa, *Chem. Phys. Lett.*, 1982, **87**, 30–33.
7 D. H. Barich, J. M. Davis, L. J. Schieber, M. T. Zell and E. J. Munson, *J. Pharm. Sci.*, 2006, **95**, 1586–1594.
8 A. J. Robbins, W. T. K. Ng, D. Jochym, T. W. Keal, S. J. Clark, D. J. Tozer and P. Hodgkinson, *Phys. Chem. Chem. Phys.*, 2007, **9**, 2389–2396.
9 U. Schwerk, D. Michel and M. Pruski, *J. Magn. Reson., Ser. A*, 1996, **119**, 157–164.
10 S. Dugar, R. Fu and N. S. Dalal, *J. Phys. Chem. B*, 2012, **116**, 9215–9222.
11 S. K. Vasa, H. Janssen, E. R. H. Van Eck and A. P. M. Kentgens, *Phys. Chem. Chem. Phys.*, 2011, **13**, 104–106.
12 V. E. Zorin, S. P. Brown and P. Hodgkinson, *J. Chem. Phys.*, 2006, **125**, 144508.
13 G. Mali, J. Trebosc, C. Martineau and M. Mazaj, *J. Phys. Chem. C*, 2015, **119**, 7831–7841.
14 W. Liu, W. D. Wang, W. Wang, S. Bai and C. Dybowski, *J. Phys. Chem. B*, 2010, **114**, 16641–16649.
15 L. M. Ryan, R. E. Taylor, A. J. Paff and B. C. Gerstein, *J. Chem. Phys.*, 1980, **72**, 508–515.
16 T. Kobayashi, K. Mao, P. Paluch, A. Nowak-Krol, J. Sniechowska, Y. Nishiyama, D. T. Gryko, M. J. Potrzebowski and M. Pruski, *Angew. Chem., Int. Ed.*, 2013, **52**, 14108–14111.
17 Y. Nishiyama, *Solid State Nucl. Magn. Reson.*, 2016, **78**, 24–36.
18 G. Kervern, G. Pintacuda, Y. Zhang, E. Oldfield, C. Roukoss, E. Kuntz, E. Herdtweck, J. M. Basset, S. Cadars, A. Lesage, C. Coperet and L. Emsley, *J. Am. Chem. Soc.*, 2006, **128**, 13545–13552.
19 E. Salager, G. M. Day, R. S. Stein, C. J. Pickard, B. Elena and L. Emsley, *J. Am. Chem. Soc.*, 2010, **132**, 2564–2565.
20 J. C. Burley, M. J. Duer, R. S. Stein and R. M. Vrcelj, *Eur. J. Pharm. Sci.*, 2007, **31**, 271–276.
21 N. J. Vigilante and M. A. Mehta, *Acta Crystallogr., Sect. C: Struct. Chem.*, 2017, **73**, 234–243.
22 A. Samoson, T. Tuherm and Z. Gan, *Solid State Nucl. Magn. Reson.*, 2001, **20**, 130–136.
23 A. A. Maudsley, A. Wokaun and R. R. Ernst, *Chem. Phys. Lett.*, 1978, **55**, 9–14.
24 D. P. Weitekamp, J. R. Garbow, J. B. Murdoch and A. Pines, *J. Am. Chem. Soc.*, 1981, **103**, 3578–3579.
25 J. R. Garbow, D. P. Weitekamp and A. Pines, *J. Chem. Phys.*, 1983, **79**, 5301–5310.
26 M. Gochin, D. P. Weitekamp and A. Pines, *J. Magn. Reson.*, 1985, **63**, 431–437.
27 B. H. Ruessink, F. J. J. Dekanter and C. Maclean, *J. Magn. Reson.*, 1985, **62**, 226–234.
28 L. D. Hall and T. J. Norwood, *J. Chem. Soc., Chem. Commun.*, 1986, 1508–1510.
29 L. D. Hall and T. J. Norwood, *J. Magn. Reson.*, 1986, **69**, 397–402.
30 L. D. Hall and T. J. Norwood, *J. Magn. Reson.*, 1986, **67**, 382–385.
31 L. D. Hall and T. J. Norwood, *J. Am. Chem. Soc.*, 1987, **109**, 7579–7581.
32 S. Vathyam, S. Lee and W. S. Warren, *Science*, 1996, **272**, 92–96.
33 J. J. Balbach, M. S. Conradi, D. P. Cistola, C. G. Tang, J. R. Garbow and W. C. Hutton, *Chem. Phys. Lett.*, 1997, **277**, 367–374.
34 W. S. Warren, S. Ahn, M. Mescher, M. Garwood, K. Ugurbil, W. Richter, R. R. Rizi, J. Hopkins and J. S. Leigh, *Science*, 1998, **281**, 247–251.
35 Y. Y. Lin, S. Ahn, N. Murali, W. Brey, C. R. Bowers and W. S. Warren, *Phys. Rev. Lett.*, 2000, **85**, 3732–3735.
36 W. Richter, M. Richter, W. S. Warren, H. Merkle, P. Andersen, G. Adriany and K. Ugurbil, *Magn. Reson. Imaging*, 2000, **18**, 489–494.
37 D. Sakellariou, S. P. Brown, A. Lesage, S. Hediger, M. Bardet, C. A. Meriles, A. Pines and L. Emsley, *J. Am. Chem. Soc.*, 2003, **125**, 4376–4380.
38 S. Cadars, A. Lesage and L. Emsley, *J. Am. Chem. Soc.*, 2005, **127**, 4466–4476.
39 I. Fugariu, W. Bermel, D. Lane, R. Soong and A. J. Simpson, *Angew. Chem., Int. Ed.*, 2017, **56**, 6324–6328.
40 B. Elena, G. de Paepe and L. Emsley, *Chem. Phys. Lett.*, 2004, **398**, 532–538.
41 G. A. Morris, H. Barjat and T. J. Home, *Prog. Nucl. Magn. Reson. Spectrosc.*, 1997, **31**, 197–257.
42 K. F. Sheberstov, D. O. Sinitsyn, D. A. Cheshkov and D. Jeannerat, *J. Magn. Reson.*, 2017, **281**, 229–240.
43 P. C. A. van der Wel, K. N. Hu, J. Lewandowski and R. G. Griffin, *J. Am. Chem. Soc.*, 2006, **128**, 10840–10846.
44 A. J. Rossini, A. Zagdoun, F. S. Hegner, M. Schwarzwälder, D. Gajan, C. Copéret, A. Lesage and L. Emsley, *J. Am. Chem. Soc.*, 2012, **134**, 16899–16908.
45 O. Lafon, A. S. L. Thankamony, T. Kobayashi, D. Carnevale, V. Vitzthum, I. I. Slowing, K. Kandel, H. Vezin, J. P. Amoureux, G. Bodenhausen and M. Pruski, *J. Phys. Chem. C*, 2013, **117**, 1375–1382.

46 A. J. Rossini, C. M. Widdifield, A. Zagdoun, M. Lelli, M. Schwarzwälder, C. Copéret, A. Lesage and L. Emsley, *J. Am. Chem. Soc.*, 2014, **136**, 2324–2334.
47 A. Zagdoun, G. Casano, O. Ouari, M. Schwarzwälder, A. J. Rossini, F. Aussenac, M. Yulikov, G. Jeschke, C. Copéret, A. Lesage, P. Tordo and L. Emsley, *J. Am. Chem. Soc.*, 2013, **135**, 12790–12797.
48 A. Zagdoun, A. J. Rossini, D. Gajan, A. Bourdolle, O. Ouari, M. Rosay, W. E. Maas, P. Tordo, M. Lelli, L. Emsley, A. Lesage and C. Copéret, *Chem. Commun.*, 2012, **48**, 654–656.
49 K. R. Mote, V. Agarwal and P. K. Madhu, *Prog. Nucl. Magn. Reson. Spectrosc.*, 2016, **97**, 1–39.
50 M. E. Halse and L. Emsley, *J. Phys. Chem. A*, 2013, **117**, 5280–5290.
51 M. Leskes, S. Steuernagel, D. Schneider, P. K. Madhu and S. Vega, *Chem. Phys. Lett.*, 2008, **466**, 95–99.
52 X. Lu, O. Lafon, J. Trébosc, A. S. L. Thankamony, Y. Nishiyama, Z. Gan, P. K. Madhu and J.-P. Amoureux, *J. Magn. Reson.*, 2012, **223**, 219–227.
53 P. J. Wheatley, *J. Chem. Soc.*, 1964, 6036–6048.
54 A. G. Mitchell and D. J. Saville, *J. Pharm. Pharmacol.*, 1967, **19**, 729–734.
55 R. Tawashi, *Science*, 1968, **160**, 76.
56 A. D. Bond, K. A. Solanko, S. Parsons, S. Redder and R. Boese, *CrystEngComm*, 2011, **13**, 399–401.
57 C. Ouvrard and S. L. Price, *Cryst. Growth Des.*, 2004, **4**, 1119–1127.
58 D. Sperger, B. Chen, T. Offerdahl, S. Hong, L. Schieber, J. Lubach, D. Barich and E. Munson, *AAPS J.*, 2005, **7**, 1991.
59 P. Vishweshwar, J. A. McMahon, M. Oliveira, M. L. Peterson and M. J. Zaworotko, *J. Am. Chem. Soc.*, 2005, **127**, 16802–16803.
60 A. D. Bond, R. Boese and G. R. Desiraju, *Angew. Chem., Int. Ed.*, 2007, **46**, 618–622.
61 E. J. Chan, T. R. Welberry, A. P. Heerdegen and D. J. Goossens, *Acta Crystallogr., Sect. B: Struct. Sci.*, 2010, **66**, 696–707.
62 A. G. Shtukenberg, C. T. Hu, Q. Zhu, M. U. Schmidt, W. Xu, M. Tan and B. Kahr, *Cryst. Growth Des.*, 2017, **17**, 3562–3566.
63 C. J. Chang, L. E. Diaz, F. Morin and D. M. Grant, *Magn. Reson. Chem.*, 1986, **24**, 768–771.
64 L. E. Diaz, L. Frydman, A. C. Olivieri and B. Frydman, *Anal. Lett.*, 1987, **20**, 1657–1666.
65 P. Hodgkinson, *Prog. Nucl. Magn. Reson. Spectrosc.*, 2005, **46**, 197–222.
66 I. Frantsuzov, S. K. Vasa, M. Ernst, S. P. Brown, V. Zorin, A. P. M. Kentgens and P. Hodgkinson, *ChemPhysChem*, 2017, **18**, 394–405.
67 Z. Gan, I. Hung, X. Wang, J. Paulino, G. Wu, I. M. Litvak, P. L. Gor'kov, W. W. Brey, P. Lendi, J. L. Schiano, M. D. Bird, I. R. Dixon, J. Toth, G. S. Boebinger and T. A. Cross, *J. Magn. Reson.*, 2017, DOI: 10.1016/j.jmr.2017.1008.1007.
68 A. Lesage, M. Lelli, D. Gajan, M. A. Caporini, V. Vitzthum, P. Mieville, J. Alauzun, A. Roussey, C. Thieuleux, A. Mehdi, G. Bodenhausen, C. Copéret and L. Emsley, *J. Am. Chem. Soc.*, 2010, **132**, 15459–15461.
69 C. Sauvee, M. Rosay, G. Casano, F. Aussenac, R. T. Weber, O. Ouari and P. Tordo, *Angew. Chem., Int. Ed.*, 2013, **52**, 10858–10861.
70 M. Rosay, L. Tometich, S. Pawsey, R. Bader, R. Schauwecker, M. Blank, P. M. Borchard, S. R. Cauffman, K. L. Felch, R. T. Weber, R. J. Temkin, R. G. Griffin and W. E. Maas, *Phys. Chem. Chem. Phys.*, 2010, **12**, 5850–5860.
71 A. Pines, M. G. Gibby and J. S. Waugh, *J. Chem. Phys.*, 1973, **59**, 569–590.
72 E. O. Stejskal, J. Schaefer and J. S. Waugh, *J. Magn. Reson.*, 1977, **28**, 105–112.
73 O. Peersen, X. Wu, I. Kustanovich and S. Smith, *J. Magn. Reson., Ser. A*, 1993, **104**, 334–339.
74 B. M. Fung, A. K. Khitrin and K. Ermolaev, *J. Magn. Reson.*, 2000, **142**, 97–101.
75 P. Caravatti, G. Bodenhausen and R. R. Ernst, *Chem. Phys. Lett.*, 1982, **89**, 363–367.
76 J. E. Roberts, S. Vega and R. G. Griffin, *J. Am. Chem. Soc.*, 1984, **106**, 2506–2512.
77 J. Clark Stewart, D. Segall Matthew, J. Pickard Chris, J. Hasnip Phil, I. J. Probert Matt, K. Refson and C. Payne Mike, *Z. Kristallogr. – Cryst. Mater.*, 2005, **220**, 567.
78 J. P. Perdew, K. Burke and M. Ernzerhof, *Phys. Rev. Lett.*, 1996, **77**, 3865–3868.
79 D. Vanderbilt, *Phys. Rev. B: Condens. Matter Mater. Phys.*, 1990, **41**, 7892–7895.
80 C. J. Pickard and F. Mauri, *Phys. Rev. B: Condens. Matter Mater. Phys.*, 2001, **63**, 245101.
81 C. C. Wilson, *New J. Chem.*, 2002, **26**, 1733–1739.

